Relaxation-Time Determination from Continuous-Microwave Saturation of EPR Spectra

Anders Lund,[a,1] Einar Sagstuen,[b] Audun Sanderud[b,c] and Jean Maruani[d]

[a] Department of Physics, Chemistry and Biology, Linköping University, S-581 83 Linköping, Sweden; [b] Department of Physics, University of Oslo, N-0316 Oslo, Norway; [c] Faculty of Health Sciences, Oslo University College, N-0130 Oslo, Norway; and [d] Laboratoire de Chimie Physique-Matière et Rayonnement, CNRS & UPMC, Curie, 75005 Paris, France

Lund, A., Sagstuen, E., Sanderud, A. and Maruani, J. Relaxation-Time Determination from Continuous-Microwave Saturation of EPR Spectra. *Radiat. Res.* 172, 753–760 (2009).

Based on the theories of Portis and of Castner 50 years ago, different continuous-wave measurement procedures for analyzing the microwave saturation power dependence of inhomogeneously broadened EPR lines were developed. Although these procedures have been refined, they still use only a few selected points on the saturation curve. A non-linear least-squares procedure for analyzing the microwave-power dependence of inhomogeneously broadened lines using all data points on a saturation curve has been developed. This procedure provides a simple alternative method to obtain magnetic relaxation data when the more direct pulse-saturation techniques are not available or are less suitable. The latter includes applications of quantitative EPR such as dosimetry. Then microwave saturation data should be obtained under conditions similar to those used in the quantitative measurements, which are usually made on first derivative spectra recorded using continuous-wave spectrometers. Selected applications to benchmark literature data and within the field of EPR dosimetry are discussed. The results obtained illustrate that relaxation times comparable to those yielded by various pulse-saturation EPR techniques can be obtained. It appears as a systematic feature that, whenever the pulse EPR data are fitted using bi-exponential functions, the shortest relaxation times obtained are those that correspond best to those measured using the current continuous-wave saturation method. © 2009 by Radiation Research Society

INTRODUCTION

The theory of continuous-wave (CW) saturation for homogenously and inhomogeneously broadened magnetic resonance lines of paramagnetic systems was developed many years ago (*1, 2*). This theory provides an alternative procedure to obtain magnetic relaxation data when the more direct pulse-saturation methods are not available or are less suitable. The latter includes

[1] Address for correspondence: Department of Physics, Chemistry and Biology, Linköping University, S-581 83 Linköping, Sweden; e-mail: ald@ifm.liu.se.

applications of quantitative EPR such as dosimetry. Then microwave saturation data should be obtained under conditions similar to those used in the quantitative measurements, which are usually made on first derivative spectra recorded using CW spectrometers.

The CW measurement procedures were later refined and employed to estimate the spin-lattice and spin-spin relaxation times, T_1 and T_2, from saturation curves in various model cases involving inhomogeneous broadening (*3–16*). The saturation parameters and relaxation times were obtained by employing diagrams that used only a few selected points on the saturation curve. Marrale *et al.* (*17*) employed an iterative fitting procedure to analyze the saturation behavior of irradiated ammonium tartrate. However, to our knowledge, a least-squares analysis making use of all data points on a saturation curve has not been proposed previously. In the present work, we developed and applied a computer program to analyze the microwave power dependence of inhomogeneously broadened lines by least-squares fitting all of the data points on a saturation curve.

LINE-SHAPE THEORY

For an inhomogeneously broadened EPR line modeled by a Gaussian envelope of Lorentzian spin packets (*1, 2*), previous treatments have shown that the line shape can be expressed in the form (*2, 6–8*)

$$g(r) \propto \frac{B_0 \beta}{\Delta B_G} \int_{-\infty}^{\infty} \frac{e^{-(a^2 r'^2)} dr'}{t^2 + (r - r')^2}, \qquad (1)$$

which is a convolution of Gaussian and Lorentzian shapes resulting in a Voigt profile. Here β is the effective transition probability of the line $g(r)$ centered at field B_0. The variables r and r' are defined respective to the corresponding magnetic fields B and B' as (*6–8*)

$$r = \frac{B - B_0}{\Delta B_L}; \quad r' = \frac{B' - B_0}{\Delta B_L}. \qquad (2)$$

The parameters a and t affecting the shape of the saturation curve are given by (2)

$$a = \frac{\Delta B_L}{\Delta B_G}; \quad t^2 = 1 + \gamma^2 B_1^2 \beta T_1 T_2 = 1 + s^2. \quad (3)$$

Here ΔB_L and ΔB_G are the widths of the unsaturated Lorentzian and Gaussian shapes, respectively, and can be expressed in terms of the peak-to-peak widths λ_L and λ_G of the corresponding first derivatives as (6–8)

$$\Delta B_L = \left(\sqrt{3}/2\right)\lambda_L; \quad \Delta B_G = \lambda_G/\sqrt{2}. \quad (4)$$

The saturation factor s contains the gyromagnetic ratio $\gamma = g\mu_B/\hbar$, the amplitude B_1 of the rotating magnetic component of the microwave field in the cavity, and the spin-lattice and spin-spin relaxation times T_1 and T_2. Note that the amplitude B_1 is one-half that of the linearly polarized field B_1^c in the resonator as used experimentally. The spin-spin relaxation time T_2 is defined as $1/\gamma\Delta B_L = 2/\gamma\lambda_L\sqrt{3}$, while the spin-lattice relaxation time T_1, which follows from Eq. (3), depends on the computation of the field B_1 from the input microwave power P.

The value of B_1 at the sample position in a microwave resonator is related to the value of P by the expression (2)

$$B_1 = k\sqrt{Q_L P} = K\sqrt{P}, \quad (5)$$

where the constant K depends on the type of resonator and on its quality factor Q_L with the sample in place (loaded Q). It may often be difficult to estimate its value with accuracy.[2]

Substituting the experimentally measured microwave power P and introducing the spin-relaxation-dependent parameter

$$P_0 = \frac{1}{K^2\gamma^2\beta T_1 T_2}, \quad (6)$$

the absorption line shape given by Eq. (1) can be recast into the condensed form (6–8, 18)

$$g(r) \propto \frac{\beta\sqrt{P}}{t} u(ar, at), \quad (7)$$

where $t = \sqrt{1 + P/P_0}$ and $u(ar, at)$ is the real part of the complex error function $w(z)$:

$$w(z) = \exp\left(-z^2\right) erfc(-iz) \; (w = u + iv, z = at + iar).$$

[2] K values for commercial cavities can be obtained from the producer or from the literature. They are often referred to a specific Q_L value and must be corrected by a factor $(Q_{Lx}/Q_L)^{1/2}$ if the actual Q_L value, Q_{Lx}, is significantly different from the reference value Q_L. For a standard rectangular TE$_{102}$ cavity (e.g. Varian, Bruker Biospin), $K^c \approx$ 0.044 mT/mW$^{1/2}$ for a Q_L value of 2500. For critically coupled cavities, the unloaded Q value, $Q_u \approx 2 \, Q_L$.

At an applied microwave power $P = P_0$, the conventional saturation parameter becomes $s = 1$. P_0 is referred to as the microwave power at saturation in the following.

The procedure to compute the line shape function $g(r)$ by expressing the function $u(ar, at)$ as the real part of the complex error function $w(z)$ (6–8) has been used in previous work (18) and will be used in the present work. The subroutine used is a FORTRAN translation of an ALGOL algorithm based on Gautschi's theory of $w(z)$ (19, 20). To measure the saturation behavior of a single, inhomogeneously broadened line, the transition probability β is set to 1, as in simple two-level systems (6–13). What is recorded experimentally is the first derivative of the absorption spectrum, and then the function $g(r)$ has to be differentiated with respect to the variable r (the magnetic field). This may be done analytically (17, 18, 21), but it was found more convenient to compute it numerically in this work.

The above model of inhomogeneous broadening, a (Gaussian) juxtaposition of (Lorentzian) spin packets, implies that, under saturation, a spin temperature (different from the lattice temperature) sets up much before spin-lattice relaxation takes place; that is,

$$T_2 \ll T_1. \quad (8)$$

If this condition is not fulfilled, then spectral diffusion from the saturated (resonant) spin packet to neighboring (non-resonant) spin packets takes place, with a cross-relaxation time T_{12}. The implications of this phenomenon (9) have been investigated in both slow and rapid CW (10, 11) and pulse (12, 13) saturation cases: $T_{12} > T_2$ and $T_{12} < T_2$, respectively.

In addition to this physical condition, which is determined by the system investigated, there is an instrumental condition that must be fulfilled so that the first derivative of the saturated line shape properly reflects the saturation of the absorption: the slow-passage condition.

Slow-Passage Condition

It is of major importance that the saturation curves are recorded under slow-passage conditions, under which the time between the field modulation cycles (assuming that the field-sweep rate is much slower than the modulation frequency) is sufficiently long for each spin packet to relax between cycles. The spin system is then continually in thermal equilibrium and the true line shape is observed. A convenient formulation of the slow-passage condition is (2, 5, 15)

$$\omega_m B_m \ll \lambda_L/T_1, \quad (9)$$

where ω_m is the modulation angular frequency and B_m is the modulation amplitude. Equation (9) intuitively

expresses that the modulation rate must be much smaller than the relaxation rate. Typical values may be $\lambda_L = 0.01$ mT, $T_1 = 10$ μs and $B_m = 0.1$ mT, requiring the modulation frequency $\nu_m = \omega_m/2\pi$ to be less than 1.5 kHz, a condition that is often difficult to achieve with many spectrometers.

Programming Details

The above formulae were incorporated in a non-linear least-squares automatic fitting computer program developed for this purpose. The input parameters to the program consist of an array of (normalized) experimental EPR signal first-derivative peak-to-peak EPR signals against microwave power together with initial trial parameter values for the Lorentzian (λ_L) and Gaussian (λ_G) linewidths and for the microwave power (P_0) at saturation. A non-linear least-squares fit of the calculated saturation curve to experimental data is performed. The code for obtaining the fitted curve was developed for the present work, while the routines for the least-squares fit were adapted from ref. (22). The output data consist of files of resulting parameter values with fitting error estimates, the experimental data and the fitted saturation curve. There is also an output file showing the calculated (isotropic) line width variation with the microwave power.[3] To conform to general practice, the saturation curves are presented as the first-derivative peak-to-peak deflection of the EPR as a function of the square root of the microwave power.

The output parameters are the microwave power (P_0) at saturation, the Lorentzian (λ_L) and the Gaussian (λ_G) line widths. T_2 is derived directly from λ_L. T_1 is calculated using the additional input of the cavity constant K. Supplying the field modulation parameters (frequency and amplitude[4]), the slow-passage condition in Eq. (9) is evaluated and compared with the modulation field settings.

To make use of previously developed code (16–18, 22), the program was written in FORTRAN. One may note that the convolution defining the Voigt profile [Eq. (1)] is computed with a single command in several high-level programming languages that also provide tools for non-linear least-squares fitting of the model to experimental data. The full source code can be provided to help conversion to e.g. Matlab code. An executable version of the program (ML_Fit11a.for/.exe) may be obtained from the authors upon request.

[3] Asymmetric contributions to the line width of a polycrystalline sample as due, e.g., to anisotropy of the g factor are not accounted for here.

[4] Note that commercial spectrometer producers conventionally quote modulation amplitudes as the peak-to-peak modulation width (deflection) and not the true amplitude.
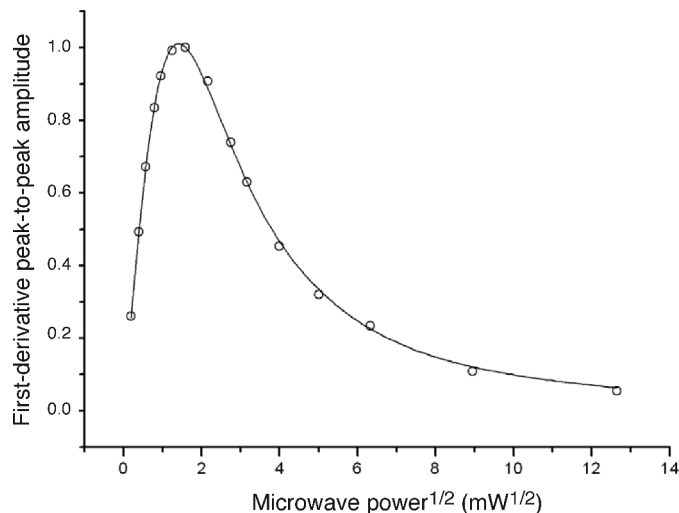

FIG. 1. Experimental data (○) (23) and fitted saturation curve for a sample calculation of T_1 and T_2 by the continuous-microwave saturation method.

APPLICATIONS

The procedure described above provides an alternative method to obtain magnetic relaxation data in such domains as quantitative EPR and its applications to dosimetry. In this section we first compare results obtained by the least-squares procedure using all points on a saturation curve with the traditional method of using a few selected points, with the example given in ref. (23). Next we consider possible applications to various materials recently suggested for EPR dosimetry applications, including 2-methylalanine (24–27). Finally a detailed line-shape analysis of the unsaturated EPR signal of the 2-methylalanine radical is performed as a consistency check of the microwave saturation analysis results.

Analysis of Example Data

We employed the raw data for the derivative peak-to-peak deflection as a function of the applied microwave power provided in ref. (23) for a model evaluation of T_1 and T_2 by the method described above. The least-squares fitting to the data (Fig. 1) gives the best-fit values and uncertainties for the saturating power (P_0) and the Lorentzian (λ_L) and Gaussian (λ_G) line widths, from which $T_2 = (0.94 \pm 0.09) \cdot 10^{-8}$ s and $T_1 = (0.90 \pm 0.38) \cdot 10^{-4}$ s are extracted, using for the factor K the value 0.031 G/(mW)$^{1/2}$ (23). The values are in good agreement with the estimate $T_1 \approx 0.88 \cdot 10^{-4}$ s, $T_2 \approx 10^{-8}$ s, as given in ref. (23).

Analysis of EPR Dosimetric Materials

The magnetic relaxation properties are of practical interest in quantitative applications of EPR such as EPR dosimetry. L-Alanine is the most widely used substance

for determining radiation doses by EPR (*28–31*). However, its EPR spectrum is composed of three different radicals (*32–35*), making this sample less suited for investigating the performance of the proposed method. Ammonium tartrate $(NH_4^+)^-OOC(CH(OH))_2$-$COO^-(NH_4^+)$ (*25, 36–38*), lithium formate, $(Li^+)H$-COO^- (*25, 39–41*), and 2-methylalanine, $H_2NC(CH_3)_2$-$COOH$ (*24–27*), have all been suggested as alternatives to L-alanine in EPR dosimetry. All have EPR spectra that are dominated by the contribution from a single radical.

The EPR spectrometer used for these experiments was a Bruker Elexsys 560 X-band instrument equipped with a Bruker ER49X SuperX microwave bridge having a Gunn diode source outputting a maximum of about 650 mW. Unless explicitly mentioned, the modulation frequency used was 750 Hz. The cavity was the Bruker standard rectangular TE_{102} cavity with a nominal conversion factor $(B_1 = K \cdot P^{1/2})$ of $K = 1.4 \ G/W^{1/2}$ at a Q value of 2500. The microwave bridge was operated without a leveler, so that the total range of microwave power within 0–50 dB attenuation for about 610 mW available power was used. Spectra were recorded at every (or every second) dB value with cavity fine tuning at each setting. In each case the peak-to-peak modulation amplitude was less than one-third of the peak-to-peak line width, the time constant less than one-tenth of the peak-to-peak scan time and the scan width covering the entire resonance line. The gain setting was adjusted so that the maximum signal did not saturate the receiver and was not changed during the experiment. The reproducibility of the data was excellent.

Ammonium tartrate. The radical $(NH_4^+)^-OOC$-$\dot{C}(OH)CH(OH)COO^-(NH_4^+)$ dominates this EPR spectrum at room temperature (*42*). The polycrystalline line shape consists of a slightly unsymmetrical single line with poorly resolved hyperfine structure and a width about 1.12 mT (*17, 25*). Due to the line-shape behavior at high microwave power, only saturation data at microwave powers below 25 mW were used (Fig. 2). The procedure described above, applied to a polycrystalline pellet irradiated with 1 kGy, gave $P_0 = (0.78 \pm 0.01)$ mW, $\lambda_L = 0.089 \pm 0.002$ mT, $\lambda_G = 1.07$ mT, $T_1 = (23.7 \pm 0.6) \cdot 10^{-6}$ s and $T_2 = (0.074 \pm 0.001) \cdot 10^{-6}$ s. Measurements on a single crystal under similar experimental conditions yielded $T_1 = (31 \pm 2) \cdot 10^{-6}$ s and $T_2 = (0.064 \pm 0.003) \cdot 10^{-6}$ s, in good agreement with the polycrystalline results. Previous pulse-EPR saturation-recovery experiments of partially deuterated ammonium tartrate crystals yielded orientation-dependent T_1 values ranging from $24 \cdot 10^{-6}$ s to $60 \cdot 10^{-6}$ s (*25*). Biexponential fitting of Carr-Purcell-Meiboom-Gill (CPMG) data gave T_M values between $0.3 \cdot 10^{-6}$ s and $1 \cdot 10^{-6}$ s, somewhat longer than the T_2 values derived in the present work. The T_M value measured by CPMG is the time constant for all processes that cause loss of spin
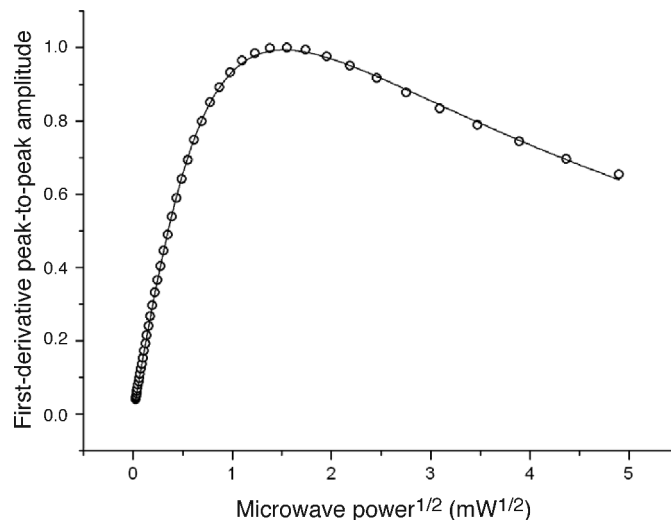

FIG. 2. Experimental data (○) and fitted saturation curve for a polycrystalline pellet of ammonium tartrate irradiated with a dose of 1 kGy. The magnetic field was modulated at 750 Hz.

coherence. The T_2 value as obtained by CW measurements is defined by means of the phenomenological Bloch equations. The T_M and T_2 values can therefore differ, but a detailed analysis of this difference is beyond the scope of this work.

Lithium formate. The $\dot{C}O_2^-$ radical anion dominates the resonance spectrum of irradiated lithium formate monohydrate samples (*41*). The line is about 1.52 mT wide for γ radiation, gradually increasing with LET up to 1.62 mT for nitrogen ions, and slightly asymmetric due to unresolved g-factor anisotropy and eight small, anisotropic hyperfine couplings to neighboring protons and lithium nuclei. As described in previous work, lithium formate pellets were exposed to different kinds of radiation (γ-ray photons, protons, neutrons and $^{14}N^{7+}$ nuclei) with doses of 20 Gy (*43*). Saturation data were recorded for each of these radiations, and the T_1 and T_2 parameters were obtained by the procedure outlined above. The results are illustrated in Fig. 3. The T_2 values vary significantly with the LET values, whereas the T_1 values were virtually constant around $0.85 \cdot 10^{-6}$ s.

These relaxation times deviate slightly from those reported earlier (*43*) due to corrections of errors in the program. Pulse-EPR data for both T_1 measurements (saturation recovery) and T_M measurements (CPMG) for lithium formate monohydrate single crystals were obtained previously (*25*). Biexponential fitting yielded the shortest relaxation times as $T_1 = 2 \cdot 10^{-6}$ s $- 3 \cdot 10^{-6}$ s and T_M about $0.5 \cdot 10^{-6}$ s, in each case three times longer than the continuous-wave experimental results.

2-Methylalanine. The radical $H_2N\dot{C}(CH_3)_2$ dominates the resonance spectrum at room temperature (*24*). The hyperfine structure due to the six quasi-equivalent protons of the two methyl groups is nearly isotropic, making this sample easier to analyze. Measurements were made on the low-field line of the derivative EPR
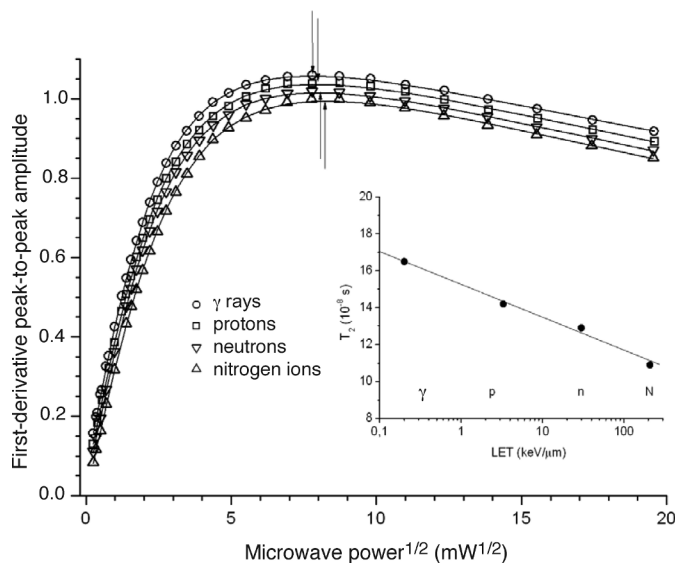
FIG. 3. Experimental data and fitted saturation curves for polycrystalline pellets of lithium formate, irradiated with a dose of 20 Gy γ rays, protons, neutrons and $^{14}N^{7+}$ nuclei. For clarity, each of the saturation curves (originally scaled to maximum at unity) is offset from the previous curve by a factor of 0.02. The power level for the maximum value of each curve is indicated by an arrow. The magnetic field was modulated at 10 kHz with a modulation peak-to-peak amplitude of 0.3 mT. With these parameters, slow-passage conditions were satisfied. The inset shows the resulting T_2 relaxation time as a function of the LET.

spectrum of a polycrystalline pellet irradiated to a dose of 1 kGy. The saturation analysis procedure described above (Fig. 4) gave $T_1 = (1.5 \pm 0.1) \cdot 10^{-6}$ s and $T_2 = (0.120 \pm 0.007) \cdot 10^{-6}$ s. Measurements on a single crystal under similar experimental conditions yielded $T_1 = (1.31 \pm 0.01) \cdot 10^{-6}$ s and $T_2 = (0.113 \pm 0.006) \cdot 10^{-6}$ s, in good agreement with the values for the pellet.
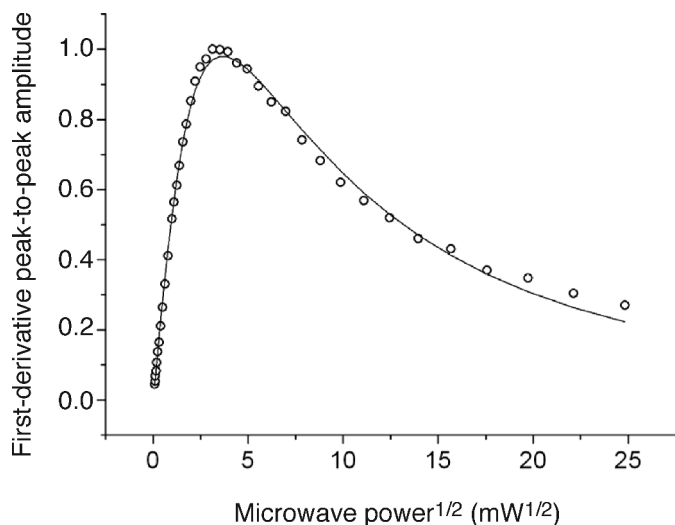

FIG. 4. Experimental data ($\bigcirc$) and fitted saturation curve for a polycrystalline pellet of 2-methylalanine irradiated with a dose of 1 kGy. The magnetic field was modulated at 750 Hz.
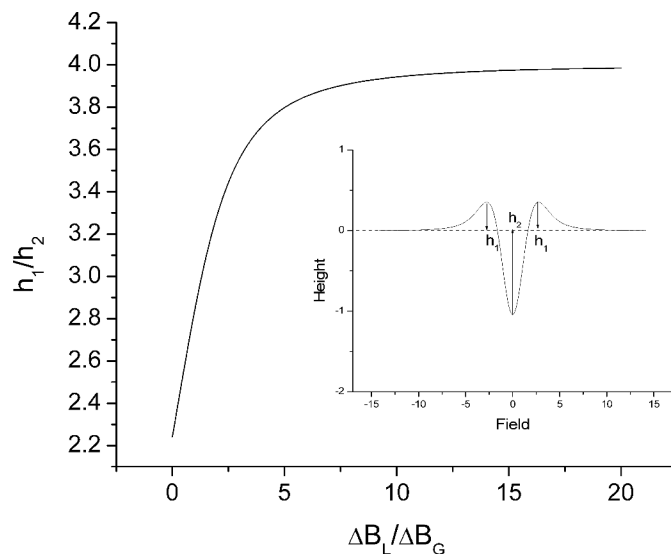

FIG. 5. The ratio $R = h_1/h_2$ for the second derivative of a Voigt profile as a function of the Lorentzian to Gaussian widths ratio $a = \Delta B_L/\Delta B_G$. The definitions of the heights h_2 and h_1 are shown in the inset.

Previous pulse (saturation recovery) EPR studies of 2-methylalanine crystals yielded an orientation-dependent value of T_1 ranging from $10 \cdot 10^{-6}$ s to $35 \cdot 10^{-6}$ s and an orientation-independent value of T_1 value of about $2 \cdot 10^{-6}$ s (24). CPMG data were scarce and yielded a rough estimate of T_M of about $0.35 \cdot 10^{-6}$ s, while Hahn echo experiments suggested a T_M value of about $0.1 \cdot 10^{-6}$ s (25).

The Unsaturated Line Shape

The analysis of saturation curves for inhomogeneously broadened lines was made under the assumption that these could be modeled by Voigt profiles. One way to test this assumption is to record the second derivative of the unsaturated resonance line (low microwave power). For a quasi-Gaussian shape, $a \ll 1$, [Eq. (3)], the ratio $R = h_2/h_1$ between the minimum and maximum amplitudes of the absorption derivative (inset of Fig. 5) approaches the value 2.24 (23), while for a quasi-Lorentzian shape, $a \gg 1$, R approaches the value 4. Between these two limits, R varies as shown in Fig. 5.

This method of analyzing the unsaturated line shape was employed, e.g., in ref. (16), but it could not be applied directly to the case of 2-methylalanine. The low-field line of the single crystal spectrum of 2-methylalanine in Fig. 6 show so-called spin-flip features (18, 45) on both sides of the main line. These features, due to dipolar hyperfine couplings with distant protons, distort the outer portions of the main line, making it difficult to estimate R for the second derivative. Similar difficulties with deducing the Lorentzian to Gaussian widths ratio from the second derivative of the unsaturated resonance line occurred for the other materials examined in this
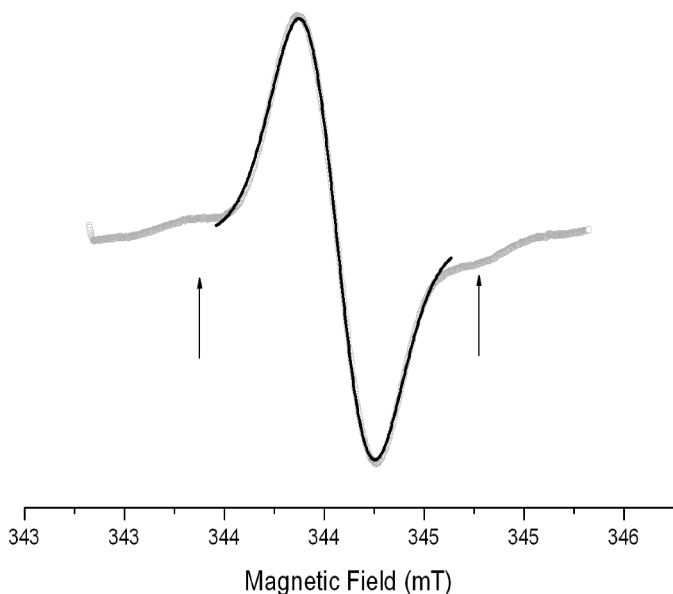
FIG. 6. Experimental (gray) and calculated (black) low-field line shapes for a single crystal of 2-methylalanine irradiated with a dose of 10 kGy and measured at 0.005 mW to avoid saturation. The calculated line shape was obtained using the least-squares method with Lorentzian and Gaussian derivative peak-to-peak widths λ_L = 0.051 ± 0.004 mT and λ_G = 0.353 ± 0.003 mT. Spectral regions affected by spin-flip lines, which are marked by arrows, were excluded from the best fit.

study. A more restricted fitting by the least-squares method to the low-field line was therefore attempted. The fit to the single crystal spectrum is shown in Fig. 6.

The derived Lorentzian derivative peak-to-peak width, λ_L = 0.051 mT, provides a value of the spin-spin relaxation time, T_2 = 0.129 · 10^{-6} s, in good agreement with the values measured on polycrystalline pellets and single crystal samples by the microwave saturation method, T_2 = (0.113−0.120) · 10^{-6} s. However, the estimate from the line shape was dependent on the assumed shape of the main line at the positions of the spin-flip features marked by arrows in Fig. 6. On the other hand, the T_2 value determined by the saturation method for a pellet was smaller by a factor of 2 than that derived for a single crystal due to larger broadening of the pellet spectrum by the g-factor anisotropy and hyperfine splittings.

DISCUSSION

The procedure developed in this work to obtain magnetic relaxation data from an analysis of the microwave power dependence of inhomogeneously broadened EPR lines using all data points on saturation curves provides an alternative method to the more direct pulse saturation techniques. The CW saturation method is particularly suited to characterize relaxation properties of samples used in applications of quantitative EPR such as dosimetry. The computer program developed in

this work to perform least-squares analysis using all points on saturation curves permits faster and more accurate analysis than the previous procedures (*5, 6, 14–17*).

Major limiting factors for the applicability of the method involve large departures of the inhomogeneous line broadening from a Gaussian shape. First, the theory does not incorporate asymmetric sources of inhomogeneous broadening such as unresolved g- and hyperfine-coupling anisotropies. Second, the anisotropic hyperfine couplings due to protons occurring in several systems are in many cases of comparable magnitude to the X-band nuclear Zeeman energy. The nuclear spins are then quantized along an effective magnetic field (*44*). This results in an inner and an outer doublet of lines for each proton (I = ½) with different intensities and different power saturation profiles. Depending on the conditions the weaker pair of lines are commonly but somewhat misleadingly referred to either as forbidden lines or as spin-flip lines (*18, 45*). Measurements at higher microwave frequencies (e.g., Q-band) may alleviate the latter factors, whereas line asymmetry due to asymmetric g anisotropy may either become resolved, thereby reducing the problem, or remain unresolved (thereby enforcing the problem). All examples presented above suffer from such distortion effects, which undoubtedly contribute to inaccuracies in the measured relaxation times. The Voigt profile assumption may also break if there is spectral diffusion through the line due to cross relaxation between the spin species (*9–13*).

Another problem is that, particularly for radicals in the solid state exhibiting EPR spectra with relatively broad lines, resonance lines from different radicals produced in different relative amounts may contribute to the line under analysis. As these different radicals exhibit different relaxation properties, the saturation curves will be distorted. For ammonium tartrate and lithium formate, for instance, this provides a significant source of uncertainty. Complementary measurements and analyses of the unsaturated line shape may in certain cases provide a value for T_2 that can be checked against the saturation method value. Such complementary measurements are best suited for isotropic systems, where the additional problems with forbidden transitions, spin-flip lines and asymmetric shapes do not occur.

The set of examples given above illustrates that in spite of these potential shortcomings of this method, relaxation times comparable to those obtained from various pulse saturation EPR methods can be obtained. It appears as a systematic feature of these results that, whenever the pulse EPR data are fitted using bi-exponential functions, the shortest relaxation times thus obtained are those that correspond best to those yielded by the current CW saturation method. The presence of an additional longer relaxation time observed in the

pulse experiments does not seem to affect the shape of the observed saturation curves and is not taken into account in the analysis.

Recently, Marrale *et al.* (*17*), presented an iterative fitting procedure based on the theory and principles used in the present work. These authors showed qualitatively, using solid-state ammonium tartrate dosimeters, that this saturation method can be used to estimate the effective LET values of the radiation. Their observations complement our results using lithium formate dosimeters (*43*), which have been extended here to include the analysis for the proton and nitrogen-ion radiations. It is clear, however, that the two methods yield very different results, because the T_2 value for 1 MeV photons at a dose of 1 kGy was $3.7 \cdot 10^{-6}$ s as reported by Marrale *et al.* (*17*), whereas the T_2 value obtained in the present work is $0.074 \cdot 10^{-6}$ s, far closer to results from pulse saturation measurements. On the other hand, the *a* values (0.04 and 0.08, respectively) and P_0 values (0.50 and 0.78, respectively) are fairly similar, as are the saturation curves. It is notable, however, that the modulation frequency of 50 kHz used by Marrale *et al.* (*17*) is far outside the slow-passage condition. The T_2 value obtained by these authors corresponds to a Gaussian line width of only 0.05 mT, according to Eq. (3). The experimental line width, close to the Gaussian-envelope line width for a Voigtian profile with predominant inhomogeneous broadening, is 1.12 mT, similar to that derived from our T_2 measurements.

REFERENCES

1. A. M. Portis, Electronic structure of F-centers: Saturation of the electron spin resonance. *Phys. Rev.* **91**, 1071–1079 (1953).

2. T. G. Castner, Jr., Saturation of the paramagnetic resonance of a V-center. *Phys. Rev.* **115**, 1506–1515 (1959).

3. J. A. Simmons, Microwave saturation in radiation-induced free radicals. *J. Chem. Phys.* **36**, 469–471 (1962).

4. O. P. Zhidkov, Y. S. Lebedev, A. I. Mikhailov and B. N. Provotorov, Deduction of relaxation parameters from saturation in non-uniformly broadened ESR lines. *Theoret. Exp. Chem.* **3**, 135–139 (1967).

5. P. R. Cullis, Electron paramagnetic resonance in inhomogeneously broadened systems: A spin temperature approach. *J. Magn. Reson.* **21**, 397–418 (1976).

6. J. Maruani, Continous saturation of "dispersion" singularities and application to molecular triplet states. *J. Magn. Reson.* **7**, 207–218 (1972).

7. J. Maruani, T. M. Kite, J-P. Korb and X. Gille, Spin relaxation of triplet pyrene in a crystal and in a glass. *Mol. Phys.* **36**, 1261–1299 (1978).

8. J-P. Korb and J. Maruani, A fast deconvolution procedure for inhomogeneous bell-shaped lines and its application to spin-relaxation studies. *J. Magn. Reson.* **46**, 514–520 (1982).

9. J-P. Korb and J. Maruani, Cross-relaxation rates and effective correlation distances for two randomly distributed dilute spin systems. *J. Chem. Phys.* **74**, 1504–1505 (1981).

10. J-P. Korb and J. Maruani, Measurement of spin-spin and spin-lattice relaxation rates for inhomogeneously broadened lines. I. Rapid spectral diffusion case. *J. Magn. Reson.* **37**, 331–348 (1980).

11. J-P. Korb and J. Maruani, Measurement of spin-spin and spin-lattice relaxation rates for inhomogeneously broadened lines. II. Slow spectral diffusion case. *J. Magn. Reson.* **41**, 247–267 (1980).

12. J-P. Korb and J. Maruani, Pulse saturation behavior of inhomogeneously broadened lines. I. Slow spectral diffusion case. *Phys. Rev. B* **23**, 971–975 (1981).

13. J-P. Korb and J. Maruani, Pulse saturation behavior of inhomogeneously broadened lines. II. Rapid-spectral-diffusion case. *Phys. Rev. B* **23**, 5700–5706 (1981).

14. M. K. Bowman, H. Hase and L. Kevan, Saturation behaviour of inhomogenously broadened EPR lines detected with magnetic field modulation. *J. Magn. Reson.* **22**, 23–32 (1976).

15. S. Schlick and L. Kevan, The application of differential saturation to distinguish radial and angular modulation mechanisms of electron spin-lattice relaxation. *J. Magn. Reson.* **22**, 171–181 (1976).

16. R. Zamoramo-Ulloa, H. Flores-Llamas and H. Yee-Madeira, Calculation of the relaxation times for an inhomogeneously broadened ESR line. *J. Phys. D Appl. Phys.* **25**, 1528–1532 (1992).

17. M. Marrale, M. Brai, A. Triolo, A. Bartolotta and M. C. D'Oca, Power saturation of ESR signal in ammonium tartrate exposed to ^{60}Co γ-ray photons, electrons and protons. *Radiat. Res.* **166**, 802–809 (2006).

18. E. Sagstuen, A. Lund, Y. Itagaki and J. Maruani, Weakly coupled proton interactions in the malonic acid radical: Single crystal ENDOR analysis and EPR simulation at microwave saturation. *J. Phys. Chem. A* **104**, 6362–6371 (2000).

19. W. Gautschi, Algorithm 363. Complex error function. *Comm. ACM* **12**, 635 (1969).

20. W. Gautschi, Efficient computation of the complex error function. *SIAM J. Num. Anal.* **7**, 187–198 (1970).

21. H. Flores-Llamas and H. Yee-Madeira, The deconvolution and evaluation of the area under ESR lines. *J. Phys. D Appl. Phys.* **25**, 970–973 (1992).

22. W. H. Press, B. P. Flannery, S. A. Teukolsky and W. T. Vetterling, *Numerical Recipes*. Cambridge University Press, Oxford, 1989.

23. C. P. Poole and H. C. Farach, *Handbook of Electron Spin Resonance*. American Institute of Physics Press, New York, 1994.

24. S. Olsson, E. Sagstuen, M. Bonora and A. Lund, EPR dosimetric properties of 2-methylalanine: EPR, ENDOR and FT-EPR investigations. *Radiat. Res.* **157**, 113–121 (2002).

25. A. Lund, S. Olsson, M. Bonora, E. Lund and H. Gustafsson, New materials for ESR dosimetry. *Spectrochim. Acta A* **58**, 1301–1311 (2002).

26. B. T. Rossi, F. Chen and O. Baffa, A new 2-methylalanine-PVC ESR dosimeter. *Appl. Radiat. Isot.* **62**, 287–291 (2005).

27. F. Chen, C. F. O. Graeff and O. Baffa, Response of L-alanine and 2-methylalanine minidosimeters for K-band (24 GHz) EPR dosimetry. *Nucl. Instrum. Methods Phys. Res. B* **264**, 277–281 (2007).

28. D. F. Regulla and U. Deffner, Dosimetry by ESR spectroscopy of alanine. *Appl. Radiat. Isot.* **33**, 1101–1114 (1982).

29. K. Mehta and R. Girzikowsky, Reference dosimeter system of the IAEA. *Radiat. Phys. Chem.* **46**, 1247–1250 (1995).

30. K. Mehta and R. Girzikowsky, IAEA high-dose intercomparison in ^{60}Co field. *Appl. Radiat. Isot.* **52**, 1179–1184 (2000).

31. D. F. Regulla, From dating to biophysics – 20 years of progress in applied ESR spectroscopy. *Appl. Radiat. Isot.* **52**, 1023–1030 (2000).

32. E. Sagstuen, E. O. Hole, S. R. Haugedal and W. H. Nelson, Alanine radicals: Structure determination by EPR and ENDOR of single crystals x-irradiated at 295 K. *J. Phys. Chem.* **A101**, 9763–9772 (1997).

33. M. Z. Heydari, E. Malinen, E. O. Hole and E. Sagstuen, Alanine radicals. 2. The composite polycrystalline alanine EPR spectrum studied by ENDOR, thermal annealing, and spectrum simulations. *J. Phys. Chem.* **A106**, 8971–8977 (2002).

34. E. Malinen, E. A. Hult, E. O. Hole and E. Sagstuen, Alanine radicals, part 4: Relative amounts of radical species in alanine dosimeters after exposure to 6–19 MeV electrons and 10 kV–15 MV photons. *Radiat. Res.* **159**, 149–153 (2003).

35. E. Malinen, M. Z. Heydari, E. Sagstuen and E. O. Hole, Alanine radicals, part 3: Properties of the components contributing to the EPR spectrum of X-irradiated alanine dosimeters. *Radiat. Res.* **159**, 23–32 (2003).

36. S. K. Olsson, E. Lund and A. Lund, Development of ammonium tartrate as an ESR dosimeter material for clinical purposes. *Appl. Radiat. Isot.* **52**, 1235–1241 (2000).

37. A. Bartolotta, M. C. D'Oca, M. Brai, V. Caputo, V. De Caro and L. I. Giannola, Response characterization of ammonium tartrate solid state pellets for ESR dosimetry with radiotherapeutic photon and electron beams. *Phys. Med. Biol.* **46**, 461–471 (2001).

38. H. Gustafsson, S. Olsson, A. Lund and E. Lund, Ammonium formate, a compound for sensitive EPR dosimetry. *Radiat. Res.* **161**, 464–470 (2003).

39. T. A. Vestad, E. Malinen, A. Lund, E. O. Hole and E. Sagstuen, EPR dosimetric properties of formates. *Appl. Radiat. Isot.* **59**, 181–188 (2003).

40. T. A. Vestad, E. Malinen, D. R. Olsen, E. O. Hole and E. Sagstuen, Electron paramagnetic resonance (EPR) dosimetry using lithium formate in radiotherapy: Comparison with thermoluminescence (TL) dosimetry using lithium fluoride rods. *Phys. Med. Biol.* **49**, 4701–4715 (2004).

41. T. A. Vestad, H. Gustafsson, A. Lund, E. O. Hole and E. Sagstuen, Radiation induced radicals in lithium formate monohydrate (LiHCO$_2 \cdot$ H$_2$O). EPR and ENDOR studies of x-irradiated crystal and polycrystalline samples. *Phys. Chem. Chem. Phys.* **6**, 3017–3022 (2004).

42. M. Brustolon, A. L. Maniero, S. Jovine and U. Segre, ENDOR and ESEEM study of the radical obtained by γ irradiation of a single crystal of ammonium tartrate. *Res. Chem. Intermed.* **22**, 359–368 (1996).

43. E. Malinen, E. Waldeland, E. O. Hole and E. Sagstuen, LET effects following neutron irradiation of lithium formate EPR dosimeters. *Spectrochim. Acta A* **63**, 861–869 (2006).

44. J. A. Weil and J. R. Bolton, *Electron Paramagnetic Resonance: Elementary Theory and Practical Applications*, 2nd ed. Wiley, New York, 2007.

45. G. T. Trammell, H. Zeldes and R. Livingston, Effect of environmental nuclei in electron spin resonance spectroscopy. *Phys. Rev.* **110**, 630–634 (1958).